

Article

Regenerative Braking Energy Flow Control Algorithm for Power Grid Voltage Stabilization in Mobile Energy Storage Systems

Ivan Župan *, Viktor Šunde , Željko Ban  and Branimir Novoselnik 

Faculty of Electrical Engineering and Computing, University of Zagreb, 10000 Zagreb, Croatia; viktor.sunde@fer.unizg.hr (V.Š.); zeljko.ban@fer.unizg.hr (Ž.B.); branimir.novoselnik@fer.unizg.hr (B.N.)

* Correspondence: ivan.zupan@fer.unizg.hr

Abstract: The paper presents a method for managing the energy storage and use of a mobile supercapacitor energy storage system (SC ESS) on a tram vehicle for the purpose of active voltage stabilization of the power grid. The method is based on an algorithm that identifies the need to utilize the energy of the SC ESS depending on changes in the voltage of the power grid caused by the driving of other nearby tram vehicles. The waveform of the current flowing into or out of the SC ESS during this control is determined based on Pontryagin's minimum principle, which optimizes the minimum change in the voltage level at the pantograph and the minimum temperature of the supercapacitor. In this way, this approach aims to minimize the changes in the voltage of the power grid caused by other vehicles and to maximize the lifespan of the supercapacitor. The algorithm was tested within the MATLAB/Simulink R2022b programming environment and experimentally validated with an HIL simulation experiment in a laboratory setup to emulate the rail vehicle system, the supercapacitor, and the power supply network.

Keywords: regenerative braking system; supercapacitor storage system; optimal control; Pontryagin's minimum principle; HIL simulation



Academic Editor: Ahmed Abu-Siada

Received: 28 November 2024

Revised: 9 January 2025

Accepted: 16 January 2025

Published: 18 January 2025

Citation: Župan, I.; Šunde, V.; Ban, Ž.; Novoselnik, B. Regenerative Braking Energy Flow Control Algorithm for Power Grid Voltage Stabilization in Mobile Energy Storage Systems. *Energies* **2025**, *18*, 410. <https://doi.org/10.3390/en18020410>

Copyright: © 2025 by the authors. Licensee MDPI, Basel, Switzerland. This article is an open access article distributed under the terms and conditions of the Creative Commons Attribution (CC BY) license (<https://creativecommons.org/licenses/by/4.0/>).

1. Introduction

The trend towards urbanization is leading to an increase in the number of passenger cars in cities and consequently to an increase in the concentration of greenhouse gases in the air. Electric rail transport is one of the solutions to this problem, as it has a lower carbon footprint. Electric rail transport and increasing its energy efficiency are among the objectives of EU directives such as the Energy Efficiency Directive and Commission Regulation 2019/1781 [1]. One of several ways to increase the energy efficiency of electric rail vehicles is the storage and subsequent use of regenerative braking energy [2–4].

The regenerative braking energy of rail vehicles is most commonly stored in battery storage systems or supercapacitors (SCs) [5,6]. Battery storage systems are characterized as having a lower number of charge and discharge cycles and a lower power density compared to supercapacitors, but batteries characteristically have a higher energy density than supercapacitors [7]. In contrast to batteries, SCs are defined by their lower energy density but have a much higher power density, as well as a larger number of charge and discharge cycles [8–10]. In urban electric rail transport, SC ESSs (supercapacitor energy storage systems) are generally chosen as a suitable ESS due to the frequent acceleration and braking processes in which high current values occur; such current values are not well suited for a battery ESS due to their aforementioned power density. The other advantage of using an SC ESS is the general simplicity of the model which lends itself to a simple

method of calculating the available energy of the ESS since the stored energy is directly proportional to its measured voltage. The position of the ESS in relation to the electric rail vehicle can influence the role that the ESS performs. The energy storage can be a mobile (onboard) or a stationary (wayside) ESS. Mobile ESSs are located in, or on, the vehicle, thus greatly reducing energy transfer losses; the generally limited remaining space in the vehicle means that it is not always possible to install an adequately sized ESS. The advantage of this type of installation is that autonomous driving is enabled, provided the energy capacity of the ESS is sufficient. The authors of [11] introduce a mixed-integer linear programming optimization to increase the utilization of regenerative braking energy in electric trains with mobile ESSs considering stochastic regenerative braking energy. Based on the expected regenerative braking energy obtained through Monte-Carlo simulations, the results present a 68.8% increase in regenerative braking energy utilization, while also reducing the expected energy drawn from the substation by 22%. The research in [12] uses a genetic algorithm with a mobile ESS to achieve a reduction in peak current values; the results show a peak current value reduction of 63.49% and substation energy savings of 15.56%. Using a mobile ESS and dynamic programming, the paper in [13] presents results of energy savings of up to 18.23% which is achieved by the objective function's weighting coefficients selection. In [14], an optimization algorithm is presented that optimizes energy savings and increases the service life of the ESS by minimizing the number of charging and discharging cycles during a tram drive. In [15], the research analyzes the economic viability of ESS installation in a vehicle. Energy savings between 5.79% and 27.83% are shown, while also showing that a 73% profit on the initial investment can be achieved over 10 years. In [16], a mixed-integer linear program is presented that takes into account various constraints of mobile ESSs such as capacity, state of charge (SoC), and aging of the ESS; depending on the observed case, the possibility of energy savings of up to 41.57% is shown. A mixed-integer linear program is also used in [17] to determine the optimal dimensions of the battery and mobile SC ESS with the aim of minimizing the long-term economic cost due to the initial cost of installing storage, energy saving, and aging components in the ESS. Depending on the ratio of the installed ESS dimensions, long-term energy savings of up to 25.59% and a reduction in investment costs per kilometer of rail vehicle travel of 3.63% are shown. The hierarchical optimal energy management of regenerative braking is presented in [18]. The algorithm enables a 10% increase in regenerative braking energy, a 10% reduction in energy losses in the system, and the potential to eliminate the braking resistor in a rail vehicle.

Stationary ESSs are commonly located near rail stops in order to minimize energy losses between the ESS and the rail vehicle; there is also the possibility for the stationary ESS to fulfill the role of active power grid voltage stabilization. The dimensioning of this type of ESS is generally designed to store a large amount of energy to cover the needs of multiple rail vehicles, but depending on the configuration of the rail route network, it is occasionally impossible to install a stationary ESS in an optimal location because the construction of such ESSs is not possible at those optimal locations. In paper [19], the problem of optimally sizing and positioning a stationary ESS is solved using a particle swarm algorithm maximizing the ROI, as well as a reduction in the power grid's total energy consumption. The rail traffic schedule optimization with a stationary ESS in [20] is carried out using a genetic algorithm, achieving an increase in energy savings of up to 17.76% depending on the traffic density of the observed railroad in Bangkok. In the paper [21], a genetic algorithm is used to optimize the speed profile of electric trains using wayside ESS to capture and reuse regenerative braking energy. The speed profile optimization aims to use braking and coasting to minimize energy consumption, taking into account the train schedule resulting in energy saving of up to 24.5% during peak hours operation. The authors of [22] analyze

the problem of optimal configuration of mobile and stationary ESSs with different storage types (SC and battery) using a mixed-integer linear program, and in simulations, a 71% reduction in the investment cost of such a regenerative braking energy storage project was achieved. The authors of [23] present a system with two installed ESSs that implement an exchange and storage of energy. The system consists of two power grid sectors powering two high-speed trains, along with compensating unwanted current waveform distortions in the three-phase power grid. A THD reduction of up to 92%, as well as a negative sequence current reduction of nearly 98%, is achieved using the presented algorithm. The genetic algorithm presented in [24] enables the utilization of up to 93.3% of the regenerative braking energy generated by using an objective function whose criterion minimizes the energy sourced from the power grid substations in conjunction with the total power grid energy losses. In [25], the research is focused on using mixed-integer linear optimization to increase energy savings with regenerative braking energy from stationary ESSs alongside photovoltaic systems, which represent supplementary energy sources, in order to analyze that system from a smart grid perspective and achieve energy savings between 16% and 35%. In [26], a strategy for transferring energy from a stationary ESS based on monitoring the state of charge depending on the daily departure schedule of rail vehicles is presented, showing a reduction in peak power of 16.3%.

Increasing the number of electric rail vehicles in cities appears to be a simple solution to reduce car emissions and traffic congestion. However, adding vehicles to the daily timetable does not necessarily go hand in hand with upgrading substations, which places an additional burden on the city's existing electric rail energy infrastructure. In practice, the power grid voltage often deviates from the nominal value due to the impact accelerations and decelerations of the rail vehicles have on the grid voltage. An additional increase in the number of vehicles on the power grid compared to the number of vehicles for which the power grid was originally planned can ultimately lead to power interruptions due to overload. Overloads occur at times when a large number of vehicles are accelerating or decelerating simultaneously in the same sector of the power grid. This can be avoided by a carefully planned schedule of vehicle departures from stations, but it is usually only feasible in the case of an underground transportation system that is not affected by other traffic (pedestrian and automobile, namely). The tram transport system is subject to the stochastic influence of other urban traffic so overloads of the power grid are sometimes unavoidable.

ESSs within the regenerative braking system of electric rail vehicles can also be used to stabilize the voltage of the power grid and reduce its peak power, thereby minimizing deviations in the voltage of the power grid. Stabilizing the power grid voltage is mostly the task of stationary ESSs unless the losses in energy storage and usage are too large or it is not possible to install the ESS in an optimal location due to lack of space in urban areas. In [27], for example, an optimization method based on successive approximation is presented that aims to regulate the voltage on rail vehicles while increasing energy savings in the power grid with reversible substations and stationary ESSs. The results show a voltage deviation reduction in the power grid from 18.5% to 44.32%. In addition, [28] presents a comparison of the effects of the particle swarm, genetic, and the fireworks algorithm, showing that each installation of stationary ESS provides a return of up to 188% of the initial investment according to the simulation results.

In this paper, which is a continuation of the research from [29], a concept of stabilizing the voltage of the tram network with the help of an ESS installed on tram vehicles, i.e., mobile ESSs, is presented. This concept is considered in order to further extend the role of mobile ESSs so that they are used as active energy sources or sinks at moments when the voltage level of the power grid changes due to the influence of other trams in the vicinity, and not only during acceleration or braking of vehicles with an installed ESS; such

situations happen when other vehicles do not have an installed ESS to reduce their impact on the power grid voltage, or when the installed ESSs in other vehicles cannot be used at that moment. Considering this approach with the research from [29] creates an opportunity to further utilize the installed ESS when it is not used during acceleration or braking, while using a similar approach for calculating the optimal ESS electric current waveform. This approach also provides an innovative way of using mobile ESSs in a functionally similar manner as stationary ESSs with regard to power grid voltage stabilization.

The chosen optimization method is based on Pontryagin's minimum principle, which optimizes between the minimum change in the voltage value at the pantograph and the minimum temperature of the SC ESS, while also taking into consideration the influence of other vehicles powered from the same power grid by measuring the voltage deviation at the pantograph of the considered electric rail vehicle. The added benefit of extending the installed SC ESS's role is to further increase energy savings and act beneficially on the power grid voltage in addition to its typical use during acceleration or braking situations while also continuing the research from [29] by optimizing power grid voltage stability with SC lifetime. Since the installed SC ESS can be used to mitigate the effect of other trams on the power grid, it also leads to the opportunity to not install SC ESSs on every tram, thereby reducing the initial capital investment. This benefit is more apparent in high-density electric rail networks such as urban tram transportation where many trams can operate in the same vicinity and locally stabilize the power grid voltage fluctuations in the same manner as a stationary ESS. The high density of electric rail vehicles also minimizes the conduction losses between them, thereby increasing energy efficiency compared to low-density rail vehicle networks where energy savings are lost due to conduction losses between vehicles.

The electric current waveform of the mobile SC ESS is based on Pontryagin's minimum principle, which optimizes the minimum change in the voltage value at the pantograph and the minimum temperature of the SC ESS, considering the influence of other vehicles powered from the same power grid. Compared to the research presented in [29], the criterion used in the calculation will be the integral square error of the power grid voltage difference between the nominal and measured voltage values. In this way, a minimization of the power grid voltage differences caused by other vehicles is achieved, as well as a maximization of the lifetime of the SC ESS on the observed vehicle by controlling its temperature, which has the greatest influence on the lifetime of the SC ESS [30,31]. In contrast to [27], the obtained optimal electric current waveform is used when the vehicle is at a standstill; the optimal current calculated in [27] is only used during acceleration and braking, resulting in the two approaches complementing each other on a functional usage level. Pontryagin's minimum principle is chosen for its ability to find the optimal input control function considering state and/or input control constraints. It is computationally more efficient than the aforementioned genetic algorithms and linear programs since the optimal input control function can generally be obtained analytically and does not necessitate searching for a solution over a large function space. Another advantage is the fact that the optimal input control function depends on the imposed system constraints, which can change frequently in urban rail transport, so the resulting input control function will change depending on the current system state and keep it optimal with regard to the chosen criterion function. The resulting optimal control variable is generally dependent on system parameters. In the case of electric rail vehicles, it is generally possible to estimate or measure them in real time, meaning that the optimal solution can be updated without the need for computationally expensive calculations as is the case with genetic algorithms. Using the concept presented in [27] and the concept presented in this paper, the combination of benefits from a mobile and a stationary ESS is achievable with respect to regenerative braking energy storage, and subsequent reuse, as well as local power grid

voltage stabilization while using a low computational complexity algorithm that calculates the optimal SC current value which also maximizes the SC lifetime.

The paper is structured as follows: In Section 2 of the paper, the regenerative braking system of the tram is presented and the mathematical models of the basic components of this system are described. In Section 3, a calculation of the optimal current of the SC ESS based on Pontryagin's minimum principle is given. In Section 4, the proposed algorithm was tested in the MATLAB/Simulink programming environment, and in Section 5, an experimental validation was carried out with an HIL simulation experiment on a laboratory setup to emulate the rail vehicle system, the SC ESS, and the power grid.

2. System Description and Mathematical Models

2.1. System Description

The tram on which the mobile SC ESS is installed has three drive bases, each with two AC traction motors with a power output of 65 kW, which are fed by a DC overhead contact line with a nominal voltage of 600 V with a tolerance of $+20/-30\%$. When the trams accelerate and brake on this power grid, currents of up to 1200 A occur, which significantly affect the voltage of the power grid. Power failures of the power grid substation occur when the voltage value is outside the tolerance range and the operation of the power grid substation is interrupted for a short time. The voltage value of the overhead contact line can increase above the maximum permissible value of 720 V in situations when several trams sharply brake within a small vicinity and no other tram can use the regenerative braking energy. For the voltage to drop below the minimum permissible value of 420 V, several nearby trams have to accelerate at the same time causing a voltage drop; this effect is intensified in uphill sections of the track if uphill driving trams accelerate at the same time. The SC consists of 4 series-connected Maxwell 125 V BMOD0165 P125 C01 supercapacitors (Maxwell, San Diego, CA, United States) with a nominal voltage of 125 V and a capacity of 63 F. A braking resistor is also installed on the tram whose role is to dissipate braking energy in situations when the power grid and the installed SC ESS are at capacity; the role of the braking resistor will not be considered in this paper. Due to the limited space in the observed tram, the installed SC occupies the remaining free space (Figure 1).

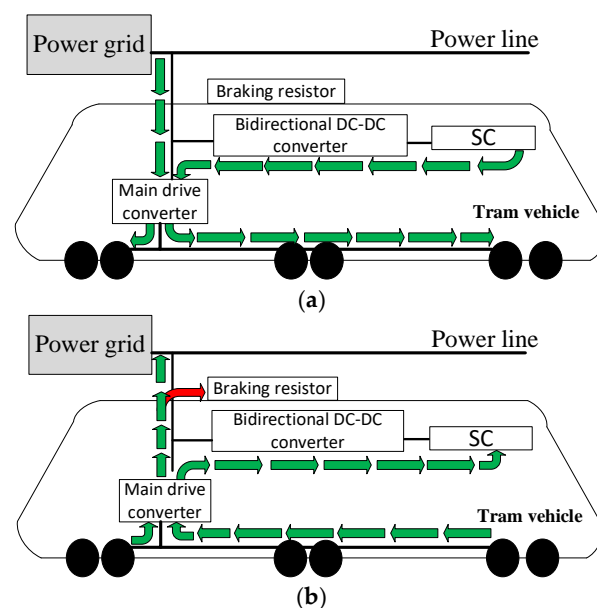


Figure 1. Regenerative braking system with energy flows displayed: (a) during acceleration and (b) during braking.

Typically, the mobile SC ESS is used as an additional energy source when accelerating the vehicle and as an energy sink when the tram is decelerating. The primary purpose of this use of the SC ESS is to reduce the energy that the vehicle draws from the power grid. Indirectly, this use of the SC ESS also reduces the vehicle's influence on the power grid voltage during acceleration and braking. However, the vehicle's SC ESS can also be used to reduce the effect of other vehicles on the power grid voltage values, such as vehicles without an installed SC ESS in situations where the vehicle under consideration with the installed SC ESS has an acceleration of zero, i.e., there is no electrical current flow in the main drive converter. In these situations, the ESS of the considered vehicle can be used as an additional source, or sink, to stabilize the voltage of the power grid that supplies the fleet consisting of vehicles with and without an installed SC ESS. The stabilization of the grid voltage can be achieved by using SC ESSs in the following ways:

- Discharging the SC of the vehicle under consideration into the grid when the voltage of the power grid is lower than the nominal value due to acceleration or constant speed driving of other vehicles in the grid.
- Charging the SC of the considered vehicle by drawing energy from the power grid when the power grid voltage has a higher value than the nominal value due to the braking of other vehicles in the grid.

The mathematical model of the system consists of three basic parts: (i) vehicle model, (ii) power grid model, and (iii) SC electrothermal model. The direction of the energy flow and the amount of energy in the SC are controlled by the developed control algorithm. The bidirectional DCDC converter connecting the SC and the main drive converter is modeled as an ideal converter since its dynamics are negligible compared to the dynamics of the algorithm. The direction of the energy flow and the amount of energy of the SC are controlled by the corresponding control algorithm. The complete system block model in MATLAB/Simulink is shown in Figure 2.

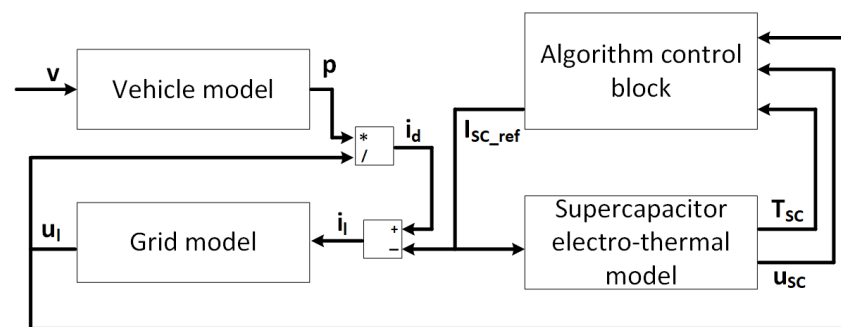


Figure 2. Block model of regenerative braking system with one rail vehicle.

The vehicle model provides the vehicle power p using the vehicle speed v as an input variable. The vehicle current i_d is calculated by dividing the provided vehicle power p with the power grid voltage u_l which is also used in the energy flow control algorithm as an input. The algorithm controls the energy flow direction of the SC depending on the value of the power grid voltage u_l and the voltage and temperature of the SC u_{SC} and T_{SC} . The output of the block that represents the algorithm is the reference current of the SC $I_{SC_{ref}}$. The difference between the vehicle current and the SC current results in the grid current i_l , which is the input for the power grid model. The input for the SC electrothermal model is the current $I_{SC_{ref}}$ and its outputs are the instantaneous SC voltage u_{SC} and the SC temperature T_{SC} .

Modeling the influence of another vehicle on the feeder network is achieved using a delay block (Figure 3). A delay of d discrete moments, i.e., z^{-d} , allows the simulation of

another vehicle nearby on the same line, in this case, another vehicle driving behind the considered vehicle. In this way, another vehicle can influence the voltage of the power grid with its driving style, and it is possible to extend the simulation model by adding more vehicles with the addition of different delay blocks which does not increase the complexity of the total model and is less memory intensive, leading to faster simulation times.

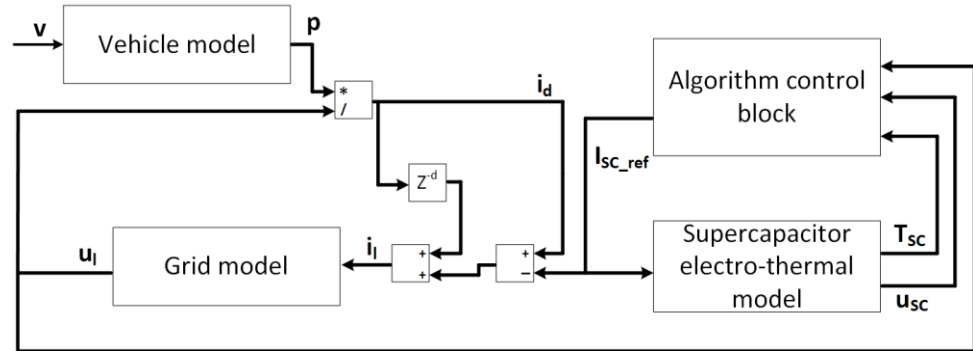


Figure 3. Block model of the regenerative braking system with two rail vehicles.

2.2. Vehicle Model

Modeling the considered tram vehicle with an installed SC ESS for simulation purposes is achieved using the Davis formula for the total traction force of the tram F_v :

$$F_v = ma + Av^2 + Bv + C + mgsin \alpha, \tag{1}$$

where

m —vehicle mass;

a —vehicle acceleration;

v —vehicle speed;

g —gravitational acceleration;

α —vehicle inline angle;

$A, B,$ and C —coefficients of the Davis formula used to model every resistive force acting on the vehicle [32].

Multiplying Equation (1) with the vehicle speed v results in the mechanical power of the vehicle P_v which is equated to the electrical power of the vehicle:

$$F_v \cdot v = u_l \cdot i_d, \tag{2}$$

where

u_l —power grid voltage, at the catenary;

i_d —vehicle current.

2.3. Power Grid Model

The model of the power grid consists of a series connection of an ideal DC voltage source U_G (voltage at the output of the power substation), power grid resistance R_l , and power grid inductance L_l . The input of the model is the power grid current i_l , and the output is the power grid voltage at the catenary, u_l :

$$u_l = U_G - i_l R_l - L_l \frac{di_l}{dt}. \tag{3}$$

The model does not take into account the distance of the considered vehicle from the power substation, or the distance between the tram vehicles, as an exact parameterization

of the power grid is not possible at this stage of the research due to the unavailability of the necessary data for that type of model. This shortcoming certainly has an impact on the resistance and inductance values of the catenary depending on the vehicle's distance from the power substation. Nevertheless, this model of the power grid can be used to draw basic conclusions about the efficiency of the developed algorithm.

The simplified model of the power grid with two tram vehicles connected to the same catenary line at the same time is shown in Figure 4. It was assumed that vehicle 1 has an SC ESS, that vehicle 2 has no SC ESS installed, and that the resistance and inductance values in the power grid model are constant.

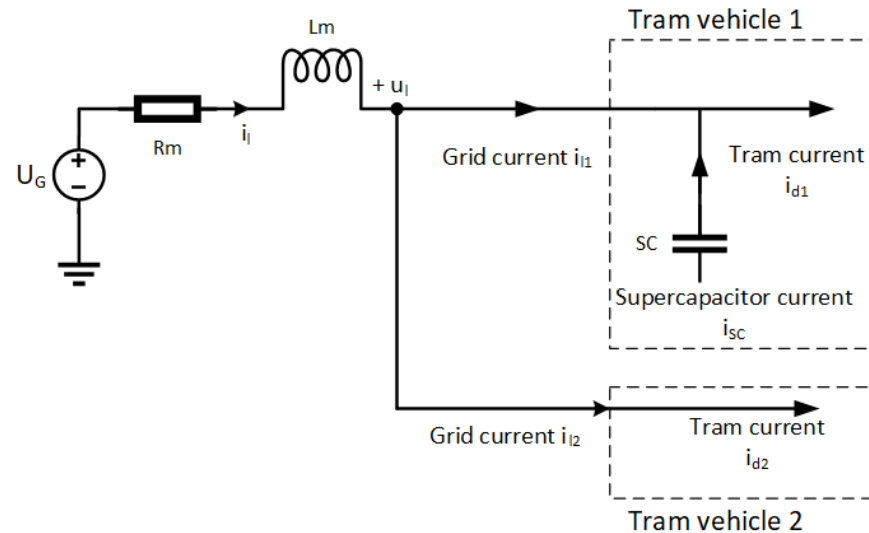


Figure 4. Model of the power grid with two tram vehicles: vehicle 1 has an SC; vehicle 2 does not have an SC.

The currents of both vehicles in Figure 4 affect the voltage u_l , which is shared by both vehicles on the same catenary line. The power grid voltage at the contact point of the catenary u_l depends on the current flowing from the substation to this catenary, i.e., it depends on the number of tram vehicles and their driving mode. The idea is to use the SC ESS outside the periods of acceleration and braking of the tram vehicle on which the SC ESS is installed in order to maintain the value of the voltage u_l at the nominal value regardless of the influence of another vehicle.

2.4. SC Electrothermal Model

The SC module electrothermal model comprises an electrical and thermal model. The electrical model of the SC is a series RC electrical circuit with capacitance C_{SC} and resistance R_{esr} ; the electrical capacitance and resistance are concentrated parameters of the connected cells within the module. This model provides the power loss P_{loss} and the SC voltage u_{SC} along with the stored energy in the SC.

Using the analogy between electrical and thermal quantities, the thermal model can be represented by elements of electrical models, such as resistances and capacitances. The thermal model of the SC consists of the thermal resistance R_{th} , thermal capacitance C_{th} , ambient temperature T_{amb} , and current source P_{loss} , which represents the thermal losses generated by the equivalent series resistance R_{esr} from the electrical model (Figure 5).

The input variable is the SC current i_{SC} , and its outputs are the SC voltage u_{SC} and its temperature T_{SC} ; their equations are described in (4) and (5):

$$u_{SC} = -i_{SC}R_{esr} - \frac{1}{C_{SC}} \int i_{SC} dt, \quad (4)$$

$$\frac{dT_{SC}}{dt} = \frac{1}{C_{th}} \left(\frac{T_{amb} - T_{SC}}{R_{th}} + i_{SC}^2 R_{esr} \right). \quad (5)$$

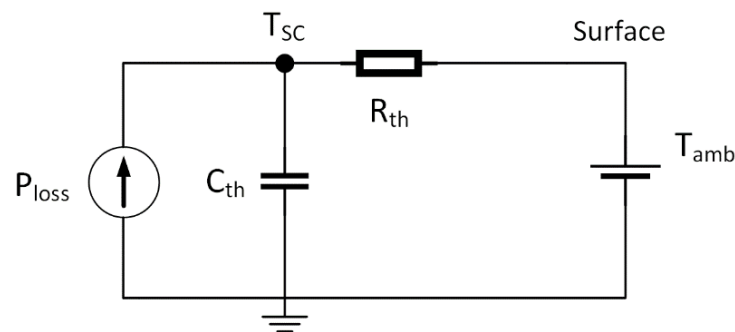


Figure 5. SC thermal model.

3. Control Algorithm and Optimal SC Current Reference Calculation

3.1. Control Algorithm

The energy control algorithm must fulfill two contradictory requirements.

The first requirement is to minimize the voltage deviation of the power grid at the catenary from its nominal value of 600 V due to the braking or acceleration of vehicles that do not have an installed SC ESS, at moments when the observed tram vehicle with SC ESS does not affect the power grid by its braking or acceleration (driving at constant speed or being at a stop). It is necessary that the state of charge of the SC enables energy to be sent to the grid or energy to be received from the grid. The maximum permissible current of the SC can be used to charge or discharge it in order to minimize deviations from the grid voltage as much as possible.

The second requirement, in contrast to the first, is to minimize the SC temperature, which increases the lifetime of the SC. To meet this requirement, the SC must be charged and discharged with as little current as possible.

The aim is to combine these two opposing requirements using Pontryagin's minimum principle in such a way that a tram vehicle with an SC ESS reduces the influence of other vehicles without an SC ESS on the power grid voltage while at the same time taking into account the preservation of the service life of its SC.

3.2. Calculation of the Optimal SC Reference Current

In this paper, Pontryagin's minimum principle is used for the optimal SC current calculation. The main reason for using Pontryagin's minimum principle is that it is possible to calculate the optimal waveform of the control variables in the general case, even in cases where control or state variables have imposed constraints. A further benefit is that the parameters of the system can change with time (or due to other dependencies) so that the subsequent usage of the principle generates a new optimal control variable waveform, taking into account changes in the parameters. A disadvantage of Pontryagin's minimum principle is its application in complex systems where the analytical solution is not possible to be calculated directly. For this reason, in this paper, in order to simplify the calculation of the optimal SC current, the regenerative braking system model is simplified as follows: (i) the power grid is represented by an ideal power source in the model, which, together with the SC, covers the energy demand of the vehicle at any time, and (ii) the influence of resistance R_{esr} on the SC voltage u_{SC} is neglected, but its influence on the SC temperature is taken into account. The calculation is explained in more detail in [27], with the main difference being the use of the integral square of power grid voltage difference in the integral part of the criterion.

The idea is to apply a criterion function that minimizes the square of the difference between the ideal value of the power grid voltage at the catenary U_m and the actual power grid voltage at the catenary u_l , together with the final SC temperature multiplied by the coefficient K_T , in order to increase the lifetime of the SC:

$$J(i_{SC}) = K_T T_{SC}(t_b) + \int_0^{t_b} (U_m - u_l)^2 dt. \quad (6)$$

The coefficient K_T is used because the value of the integral $\int_0^{t_b} (U_m - u_l)^2 dt$ can differ by several orders of magnitude from the final SC temperature $T(t_b)$. By choosing the coefficient K_T , the values of the temperature criterion and the voltage integral criterion can become equal, which ensures an equal effect on both criteria or gives one criterion the advantage over the other.

For the tram vehicle with an installed SC ESS, the state variables are as follows:

$$\frac{du_{SC}}{dt} \approx -\frac{1}{C_{sc}} i_{SC}, \quad (7)$$

$$\frac{dT_{SC}}{dt} = \frac{1}{C_{th}} \left(\frac{T_{amb} - T_{SC}}{R_{th}} + i_{SC}^2 \cdot R_{esr} \right), \quad (8)$$

$$u_l = U_G - i_l \cdot R_m - L_m \frac{di_l}{dt}, \quad (9)$$

$$i_l = i_{d1} + i_{d2} - i_{SC}. \quad (10)$$

Combining Equations (9) and (10) results in the following equation:

$$\frac{di_{d1}}{dt} + \frac{di_{d2}}{dt} + \frac{di_{SC}}{dt} = \frac{1}{L_m} (U_G - (i_{d1} - i_{SC})R_m - u_l). \quad (11)$$

Taking into account that the SC is used only when the considered tram vehicle is at a stop, or driving at a constant speed, the derivative $\frac{di_{d1}}{dt}$ is equal to zero. For the second tram vehicle, the current i_{d2} is considered to be constant at the moment $t = 0$, which results in the following:

$$\frac{di_{SC}}{dt} = \frac{1}{L_m} (U_G - (i_{d1} - i_{SC})R_m - u_l). \quad (12)$$

Since i_{SC} is the calculated control variable, it cannot be part of the differential state equations of the system.

The Hamiltonian of the system is described as follows:

$$H(T_{SC}, u_{SC}, i_{SC}, \lambda_1, \lambda_2, t) = (U_m - u_l)^2 + \lambda_1 \frac{dT_{SC}}{dt} + \lambda_2 \frac{du_{SC}}{dt}, \quad (13)$$

where $\lambda_1(t)$ and $\lambda_2(t)$ are the Lagrange multipliers of the Hamiltonian. Furthermore, the first set of conditions that must be satisfied in the Pontryagin principle is described as follows:

$$\frac{d\lambda_1}{dt} = -\frac{\partial H}{\partial T} = \frac{1}{C_{th} R_{th}} \lambda_1, \quad (14)$$

$$\frac{d\lambda_2}{dt} = -\frac{\partial H}{\partial u_{SC}} = 0, \quad (15)$$

$$\lambda_1(t_b) = \frac{\partial K}{\partial T} + q_1^o = K_T + q_1^o, \quad (16)$$

$$\lambda_2(t_b) = \frac{\partial K}{\partial u_{SC}} + q_2^o = q_2^o, \tag{17}$$

$$\lambda_1 = C_1 e^{\frac{t}{R_{th}C_{th}}}, \tag{18}$$

$$\lambda_2 = C_2 = q_2^o. \tag{19}$$

The direction of the vector $q^o = [q_1^o \ q_2^o]^T$ is equal to $[0 \ -1 \ -1]^T$ in the case where the SC is fully discharged or $q^o = [0 \ 1]^T$ in the case where the SC is fully charged; the vector can be multiplied by any scalar as long as the original direction is conserved. In other cases, q^o is a null vector.

The following inequality must be satisfied as another condition of optimality in the Pontryagin principle which ensures that the calculated SC current is always optimal:

$$H(T_{SC}^o, u_{SC}^o, i_{SC}^o, \lambda_1^o, \lambda_2^o, t) \leq H(T_{SC}^o, u_{SC}^o, i_{SC}, \lambda_1^o, \lambda_2^o, t), \tag{20}$$

$$\begin{aligned} (U_m - u_l)^2 + \lambda_1^o \frac{1}{C_{th}} \left(\frac{T_{amb} - T_{SC}^o}{R_{th}} + i_{SC}^{o2} R_{esr} \right) - \lambda_2^o \frac{1}{C_{SC}} i_{SC}^o \leq \\ (U_m - u_l)^2 + \lambda_1^o \frac{1}{C_{th}} \left(\frac{T_{amb} - T_{SC}^o}{R_{th}} + i_{SC}^2 R_{esr} \right) - \lambda_2^o \frac{1}{C_{SC}} i_{SC}, \end{aligned} \tag{21}$$

$$\begin{aligned} (U_m - u_l)^2 + \lambda_1^o \frac{1}{C_{th}} \left(i_{SC}^{o2} R_{esr} \right) - \lambda_2^o \frac{1}{C_{SC}} i_{SC}^o \leq \\ (U_m - u_l)^2 + \lambda_1^o \frac{1}{C_{th}} \left(i_{SC}^2 R_{esr} \right) - \lambda_2^o \frac{1}{C_{SC}} i_{SC}. \end{aligned} \tag{22}$$

Since an optimal SC current i_{SC}^o will minimize the Hamiltonian, the last equation can be derived with respect to i_{SC}^o and made equal to zero in order to obtain the desired SC optimal current:

$$\frac{\partial}{\partial i_{SC}^o} \left((U_m - u_l)^2 + \lambda_1^o \frac{1}{C_{th}} \left(\frac{T_{amb} - T^o}{R_{th}} + i_{SC}^{o2} R_{esr} \right) - \lambda_2^o \frac{1}{C_{SC}} i_{SC}^o \right) = 0, \tag{23}$$

$$2(U_m - u_l)(-R_m) + 2\lambda_1^o \frac{R_{esr}}{C_{th}} i_{SC}^o - \lambda_2^o \frac{1}{C_{SC}} = 0, \tag{24}$$

$$i_{SC}^o = -\frac{-2R_m(U_m - u_l) - \lambda_2^o \frac{1}{C_{SC}}}{2\lambda_1^o \frac{R_{esr}}{C_{th}}} = -\frac{-2R_m(U_m - u_l) - q_2^o \frac{1}{C_{SC}}}{2 \left(C_1 e^{\frac{t}{R_{th}C_{th}}} \right) \frac{R_{esr}}{C_{th}}}. \tag{25}$$

The resulting optimal SC current depends on the instantaneous difference in the power grid voltage from the ideal power grid voltage value. The SC current denominator contains the term $e^{\frac{t}{R_{th}C_{th}}}$ which will asymptotically send the value to zero as $t \rightarrow \infty$; the criterion for the final SC temperature $K_T T_{SC}(t_b)$ necessitates that the SC current is not a constant value through time since the SC current increases the SC temperature T_{SC} . The advantage of having an optimal SC current in this form is that the parameter variations can be updated through software calibrations or online parameter estimations, keeping the calculation of i_{SC}^o simple and computationally inexpensive compared to genetic algorithms or linear programming which would need to recalculate the optimal solution after every parameter change. By carefully choosing the value of C_1 , it is also possible to scale the value of i_{SC}^o to influence the chosen aspect of the algorithm: energy savings or SC lifetime improvement.

In order to validate the algorithm developed in this chapter, two experiments were conducted: Firstly, MATLAB/Simulink simulation environment was used to simulate the system offline. Secondly, an HIL laboratory setup was created to emulate the complete tram vehicle, SC ESS, and power grid to verify the proposed algorithm’s validity in real time.

4. Offline Simulation Experiment

4.1. Offline Simulation Model

The offline simulation experiment carried out in MATLAB/Simulink uses a model based on previously developed mathematical models of the tram vehicle, the SC electrothermal model, and the power grid model in Section 2 along with the proposed control algorithm in Section 3.

The simulation covers one tram ride on the Zagreb tram network line no.14. The experiment was conducted in such a way that two trams run on line no. 14: tram 1, which has an installed SC, and tram 2, which does not have an SC and runs with a time delay of 25 s compared to tram 1; in this way, the influence of both trams on the voltage of the power grid at the catenary can be modeled.

Line no. 14 was selected because it includes changes in altitude, more precisely, a significant ascent/descent on part of the route, which also affects the voltage of the power grid at the catenary. The simulation model in MATLAB/Simulink is shown in Figure 6. The modeling of the effects of the second tram was realized with the Transport Delay block, which allows the selection of the signal delay. In this case, the current of the second tram (without an installed SC) is 25 s behind the observed tram. The second tram uses the identical speed profile of the first tram, but with a time delay, as this approximates the driving situation of two neighboring trams in an identical traffic situation. The considered tram speed profile used in the simulation experiment, Figure 7, was determined by measurements during a two-day tram journey on line no. 14. The gradients of the railway sections are marked in the figure.

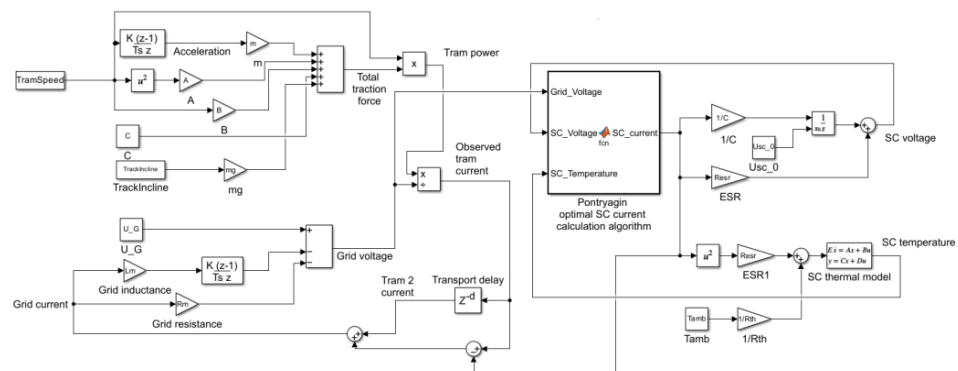


Figure 6. MATLAB/Simulink model of SC–power grid–tram system along with the control algorithm.

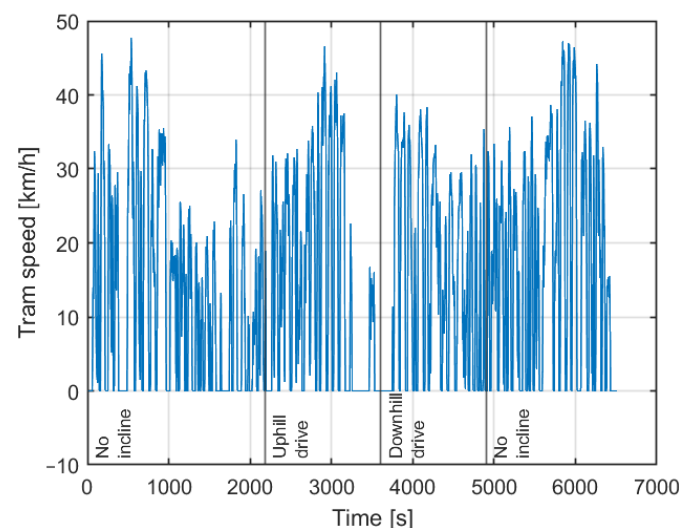


Figure 7. Speed profile of the considered tram on the Zagreb electric tram network line no. 14.

Table 1 shows the parameters for the MATLAB/Simulink simulation model.

Table 1. MATLAB/Simulink simulation parameters.

Parameter	Value	Parameter	Value
A	17.965	R_{th}	0.04 °C/W
B	34.536	C_{th}	33,000 J/°C
C	7827.249	T_{amb}	25 °C
U_G	600 V	u_{SC0}	450 V
R_l	0.0387 Ω	C_1	12,960
L_l	0.0023 H	q_2^o	20
R_{esr}	0.018 Ω	K_T	13,058
C_{SC}	63 F		

Parameters A , B , and C , as well as R_l , L_l , and U_G , were calculated from the solution of the optimization problem described in [14]. Parameters R_{esr} , C_{SC} , R_{th} , and C_{th} are from the datasheet of the supercapacitor module Maxwell 125 V Module BMOD0165 P125 C01.

Obtaining the values of parameters C_1 , q_2^o , and K_T was achieved in the following manner:

The tram acceleration time was chosen empirically to be $t_b = 10$ s. After that time has elapsed, the modeled tram current typically reaches a value of 800 A. Equating both criteria within the criterion function $J(i_{SC})$ results in the following:

$$K_T T(t_b) = \int_0^{10} (U_m - u_l)^2 dt, \quad (26)$$

giving $K_T = 13058$. Substituting this value into the following equation,

$$\lambda_1(t_b) = K_T = C_1 e^{\frac{1}{C_{th} R_{th}} t_b}, \quad (27)$$

results in $C_1 = 12960$.

The value of q_2^o is calculated from the numerator of the formula for the optimal SC current i_{SC}^o , $-2R_m(U_m - u_l) - q_2^o \frac{1}{C_{SC}}$. It is also necessary to respect the direction of q_2^o , defined in Section 3.2. In situations when the power grid voltage at the catenary has a value lower than the ideal value, i.e., $u_l < U_m$, the objective is to discharge the SC which states that $q_2^o < 0$. Discharging the SC is achieved with a positive i_{SC}^o value, which results in the following inequality:

$$i_{SC}^o = -\frac{-2R_m(U_m - u_l) - q_2^o \frac{1}{C_{SC}}}{2 \left(C_1 e^{\frac{t}{R_{th} C_{th}}} \right) \frac{R_{esr}}{C_{th}}} > 0, \quad (28)$$

The denominator of Equation (29) is always positive, because the values R_{esr} , C_{th} , and C_1 are always positive, meaning that the numerator must also always be a positive value, while also satisfying the inequalities $U_m - u_l > 0$ and $q_2^o < 0$:

$$\begin{aligned} & -\left(-2R_m(U_m - u_l) - q_2^o \frac{1}{C_{SC}}\right) > 0, \\ & -2R_m(U_m - u_l) - q_2^o \frac{1}{C_{SC}} < 0, q_2^o > -2R_m C_{SC}(U_m - u_l), \\ & -2R_m C_{SC}(U_m - u_l) < q_2^o < 0. \end{aligned} \quad (29)$$

Since the values of R_m , C_{SC} , and $U_m - u_l$ are always positive, the expression $-2R_m C_{SC} (U_m - u_l)$ will always be negative. A similar principle can be applied for the case when $U_m < u_l$, and the SC is charged from the power grid with the SC current $i_{SC}^0 < 0$:

$$-2R_m C_{SC} (U_m - u_l) > q_2^0 > 0. \quad (30)$$

Continuing on the work presented in [33], the maximum SC charging and discharging current's dependence on the instantaneous SC temperature T_{SC} is presented with the following formula:

$$i_{SC_max} = 240e^{\frac{65-T_{SC}}{K_{SC}}}. \quad (31)$$

The parameters used for (31) are as follows: at 25 °C, the maximum charging/discharging current is equal to 400 A; for the maximum SC operating temperature of 65 °C, the charging/discharging current is set to 240 A, which corresponds to the maximum operating current of the SC at the maximum operating temperature. The coefficient K_{SC} is calculated according to the following equation by setting the beforementioned values as specified:

$$\begin{aligned} 400 &= 240e^{\frac{65-25}{K_{SC}}} = 240e^{\frac{40}{K_{SC}}}, \\ \ln \frac{400}{240} &= \frac{40}{K_{SC}}, \\ K_{SC} &= \frac{40}{\ln \frac{400}{240}} = 77.999. \end{aligned} \quad (32)$$

As described in Section 3, the algorithm works as follows: if the acceleration of the tram with the installed SC is zero and if the power grid voltage is less than the nominal value of 600 V, the SC is discharged into the grid, and if the power grid voltage is greater than 600 V, the SC is charged from the grid. To avoid oscillations when switching the algorithm on and off, the following switching limits of the algorithm were selected:

- The SC is charged when the power grid voltage at the catenary exceeds 605 V until it drops to 601 V.
- The SC is discharged when the power grid voltage at the catenary falls below 580 V until it exceeds 595 V.

These switch-on and switch-off limits of the algorithm were selected based on the power grid voltage range of 420 V to 720 V. The lower limit of the mains voltage is 30% below the nominal voltage of 600 V, while the upper limit is 20% above. It is therefore obvious to emphasize the effect of the algorithm on voltage values above 600 V in order to prevent potential outages of the power substation due to overloads of the power grid. The moments of activation of the algorithm according to the specified voltage and acceleration criteria are shown in Figure 8.

If the tram fulfills the previously defined criteria for the inclusion of the algorithm at a certain point in time, the following conditions are checked in order to verify that the SC is available for use:

- If the SC voltage is in the range $< 250, 500 > V$, enable the charging/discharging of the SC.
- If the SC voltage is $\leq 250 V$, only enable the charging of the SC.
- If the SC voltage is $\geq 500 V$, only enable the discharging of the SC.

Figure 9 shows the moments during a tram drive when all conditions for switching on the energy control algorithm of the SC are met with the parameters from Table 1, where the moments of charging are marked with 1 and the moments of discharging with -1 .

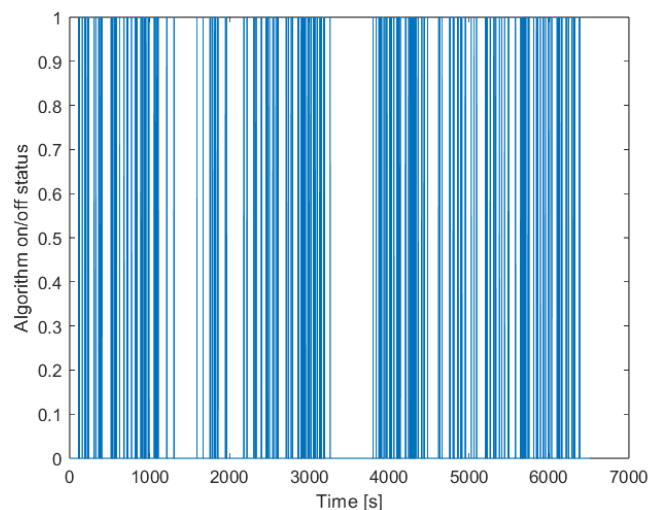


Figure 8. Activation moments for the energy control algorithm based on voltage and acceleration criteria.

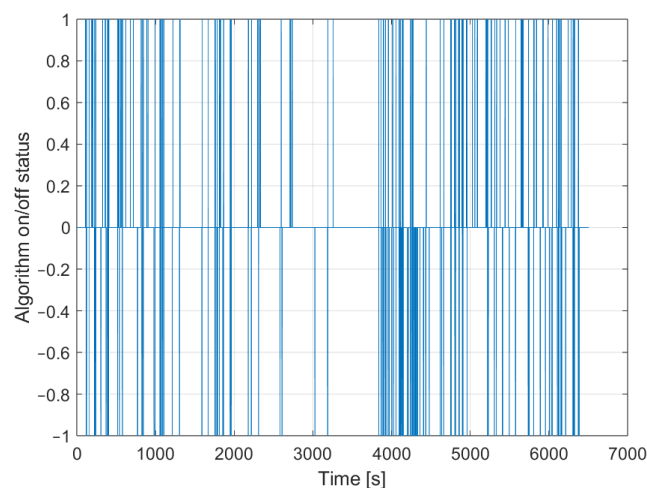


Figure 9. Moments of switching on the algorithm when all conditions are met.

4.2. Offline Simulation Experiment Results

The results of the system simulation with the proposed algorithm compared to the system without the algorithm are presented below.

Figure 10 shows the effect of the algorithm on the power grid voltage at the catenary. In the case of when the algorithm is used with the ESS, the power grid voltage values are closer to the nominal value of 600 V. Depending on the situation, it is sometimes not possible for the observed tram to act on the power grid network due to it not being stationary and/or not having enough energy stored in the SC ESS, as shown in Figure 11b. Furthermore, the calculated optimal SC current waveform has lower values than tram currents, which can be as high as 1200 A during uphill drive; higher SC current values increase the temperature of the SC ESS, shortening its lifetime.

The SC current waveform is shown in Figure 11a. According to the expression for the optimal SC current from Equation (25), its value depends mainly on the voltage difference ($U_m - u_l$), as can be seen from Figures 10 and 11: a larger voltage difference ($U_m - u_l$) produces a larger SC current, which leads to a greater reduction in the voltage difference under the action of the algorithm than when there is no algorithm. During the operation of the algorithm, the increase in the criterion $\int (U_m - u_l)^2 dt$ is reduced by up to 25% in situations where the voltage deviation of the supply network is significant, such as at the

moment when $t = 540$ s (Figure 10); by comparing the voltage waveforms, the value of the voltage deviation is reduced by 12 V.

The SC voltage waveform, which is shown in Figure 11b, shows the moments of energy exchange with the power grid. It can be seen that the SC is almost always empty during the ascent for two reasons:

1. The acceleration of the second tram on the incline requires more energy as gravity has to be compensated, causing larger voltage drops and resulting in a faster discharging of the SC.
2. Due to the influence of gravity, a smaller amount of regenerative braking energy is available to the second tram, so less energy is available to charge the SC.

On the downhill section, it can be seen that the SC voltage of the SC increases because the braking of the second tram on the downhill run increases the power grid voltage, which enables more frequent charging of the SC; this manifests itself in voltage values closer to the nominal voltage of the power grid compared to the case without the algorithm.

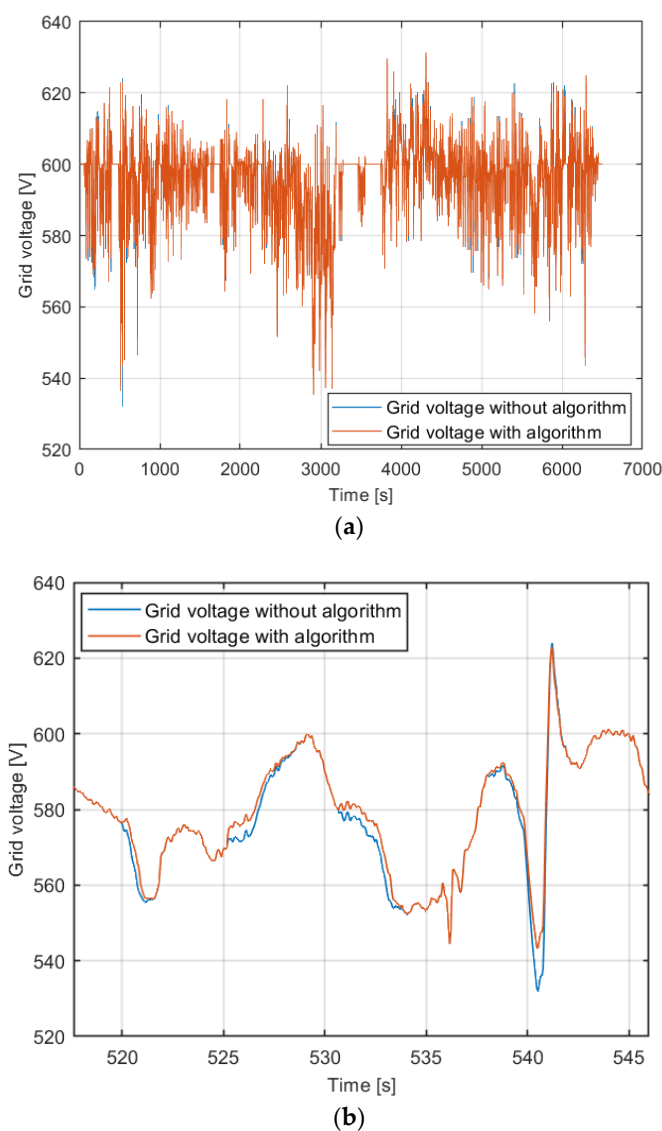


Figure 10. Power grid voltage waveform with and without the effect of the algorithm: (a) during the whole ride on line no. 14; (b) 25 s time period.

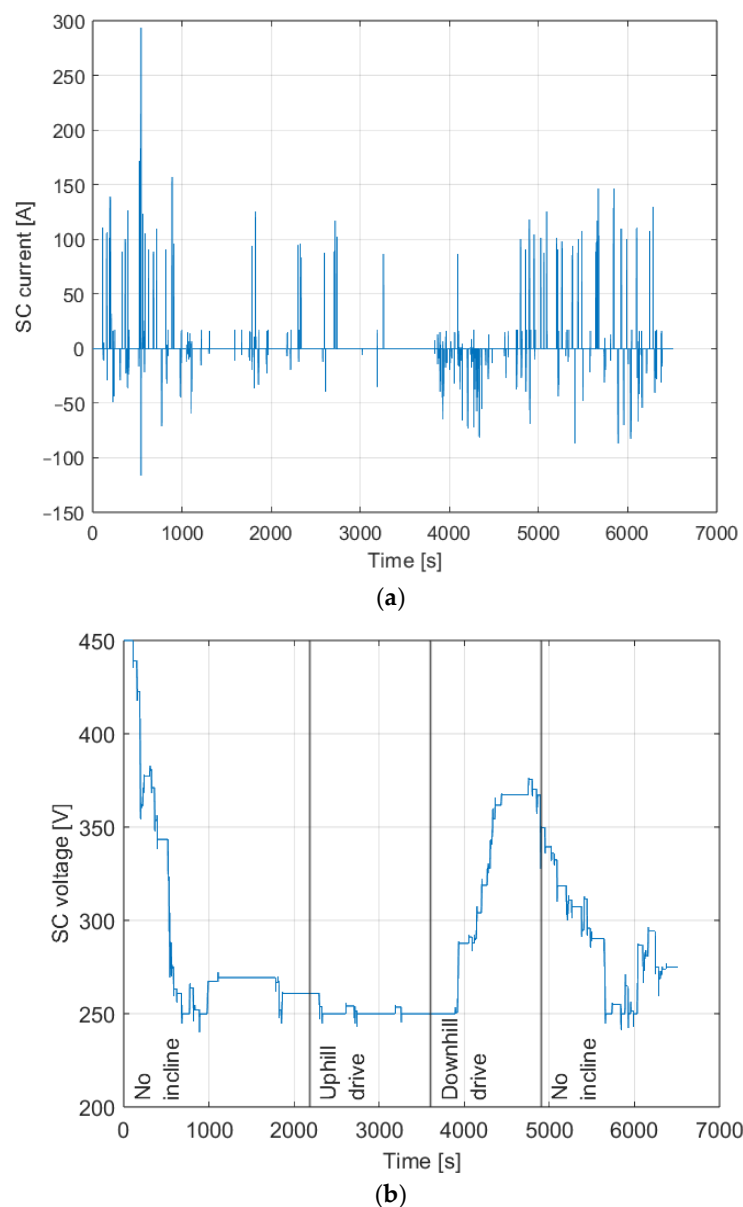


Figure 11. SC current and voltage waveform: (a) SC current; (b) SC voltage.

The SC temperature waveform shown in Figure 12 indicates that the temperature increase is minimal due to the short charging and discharging intervals. Analyzing Figure 12 alongside Figure 11 shows that the SC temperature does not increase during the uphill drive section. This behavior is fitting since the SC voltage is very low, leaving a very small amount of energy to be used during intervals when the power grid voltage is below the threshold. The SC temperature changes do not significantly shorten the SC lifetime, signifying that the proposed algorithm can be used alongside algorithms such as the one proposed in [27] and increase the power grid voltage stability. The SC temperature changes can be reduced when multiple nearby vehicles contribute to the power grid voltage stabilization.

By changing the coefficient K_T , the operation of the algorithm can be manipulated, allowing additional flexibility in the design of the regenerative braking system's energy flow control algorithm. Table 2 shows the influence of the coefficient K_T on the maximum temperature of the SC and on the amount of energy the SC received from the grid at times when the power grid voltage was above 600 V.

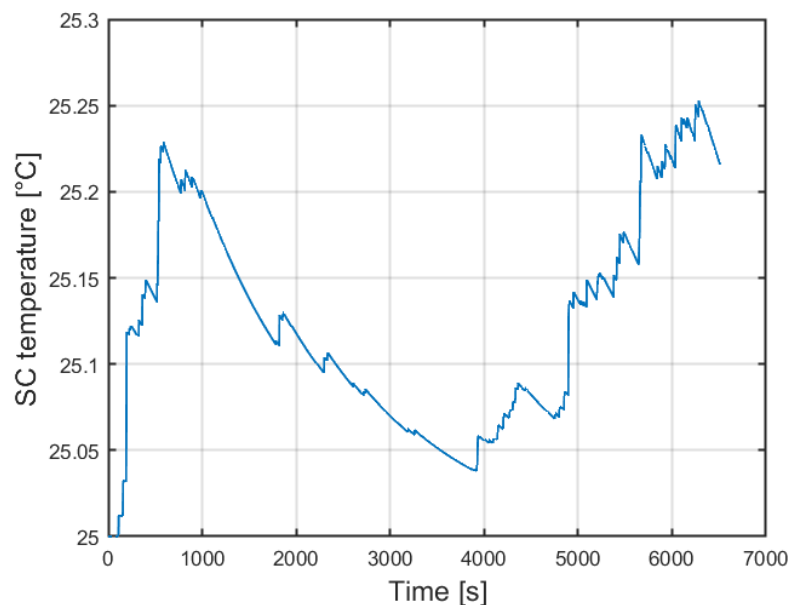


Figure 12. SC temperature waveform.

Table 2. Influence of K_T values on the SC temperature and stored energy.

K_T	Maximum Temperature	Total Stored Energy
1305.8	26.9 °C	$9.67 \cdot 10^4$ J
13,058	25.25 °C	$3.55 \cdot 10^4$ J
130,580	25.01 °C	$8.14 \cdot 10^3$ J

According to Table 2, as the value of the coefficient K_T increases, the influence of the final temperature in the criterion function of the algorithm from Equation (6) increases, i.e., the maximum temperature of the SC decreases. An increase in the influence of the temperature on the value of the criterion function leads to a smaller value of the optimal SC current from (25), since K_T appears in the denominator as $\lambda_1(t_b)$. Accordingly, the energy that the SC receives from the grid (or sends to the grid) is also reduced because the value of the SC current is smaller. The inverse is valid when the value of the K_T coefficient decreases.

The voltage stabilization benefits of the algorithm are more apparent when they are compared to the results from [27]. The algorithm presented in [27] is also based on Pontryagin's minimum principle but with a focus on energy saving during regenerative braking and its subsequent reuse during acceleration instead of voltage stabilization for the considered vehicle. The presented algorithm aims to lessen the impact of other vehicles on the power grid voltage, while the algorithm from [27] focuses only on the impact caused by itself through acceleration and braking. Figure 13 shows the power grid voltage waveform from the identical simulation environment used in this paper, but using the algorithm with its parameters presented in [27], in a time period similar to Figure 10b.

The effect of the algorithm proposed in [27] on the power grid voltage stabilization is beneficial since less energy is exchanged with the power grid during acceleration/braking of the considered vehicle, but since the algorithm does not consider the instantaneous voltage value, there are times when the algorithm is not necessarily stabilizing the power grid voltage value, shown with the dotted vertical line in Figure 13. The algorithm presented in this paper allows for a more focused approach to voltage stabilization compared to the algorithm from [27] while also showing a minimal impact on SC temperature, and consequently, SC lifetime, compared to the impact in [27], as shown in Table 3.

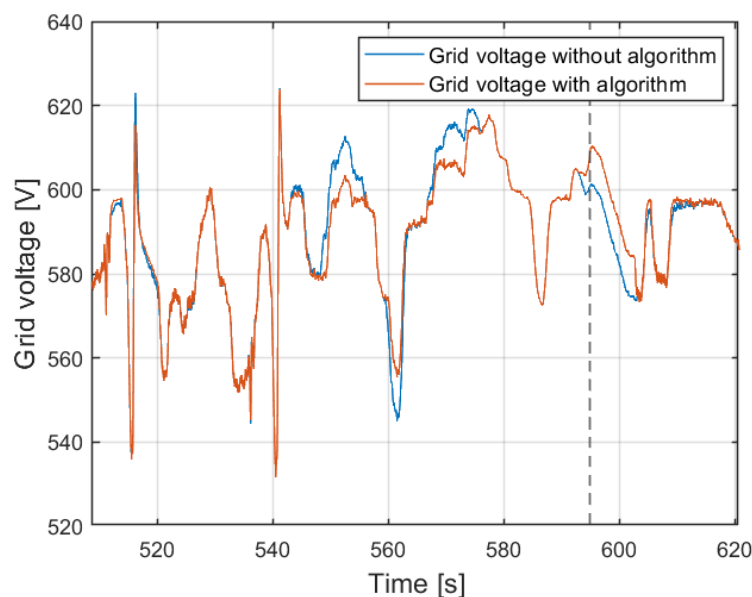


Figure 13. Power grid voltage waveform with and without the effect of the algorithm from [27] in a timescale similar to Figure 10b.

Table 3. Comparison of SC maximum temperature from proposed algorithm and [27].

K_T	Maximum SC Temperature in This Paper	Maximum SC Temperature in [27]
$K_T/10$	26.9 °C	38.18 °C
K_T	25.25 °C	37.6 °C
$K_T \cdot 10$	25.01 °C	35.36 °C

Since the approach taken in this paper is to use the SC ESS when the considered vehicle is stationary, it is not suitable for an equal comparison to the algorithm developed in [27], which is only active during the acceleration and braking of the considered tram. Instead, they complement each other's functionality by making use of the installed SC ESS on one vehicle both as a mobile and stationary ESS.

5. HIL Simulation Experiment

5.1. HIL Simulation Model

The real-time experimental verification of the functionality and validity of the developed algorithm is conducted using an HIL laboratory setup that emulates the tram–power grid–SC system used (Figure 14). In this way, the validity and functionality of the algorithm can be verified in real time without the need for testing on the real tram which achieves the physical safety of the considered tram and financial savings in the algorithm testing phase.

The previously developed mathematical models of the tram, the power grid, and the control algorithm are implemented in the Typhoon HIL 402 real-time simulation programming environment (Figure 15). The physical implementation of the calculated quantities is achieved with the Danfoss FC302 converter (Figure 14). This configuration enables each branch of the converter to act as a bidirectional DC/DC converter and, together with the associated inductor and the ESS, emulates a component of the real physical system. The converter phase connected to the Maxwell BMOD0083 P048 B01 (48 V, 83 F) supercapacitor represents the bidirectional DCDC converter and the SC; the other branches emulate the tram vehicle and the power grid connected to the LiFePO₄ batteries (36 V, 12 Ah). The

calculated values in the Typhoon HIL real-time simulator generate a 10 kHz PWM signal that controls the switches in each phase of the Danfoss FC302 converter (Danfoss, Nordborg, Denmark). The real-time closed-loop control of each phase’s current and voltage is enabled through real-time current and voltage measurements.

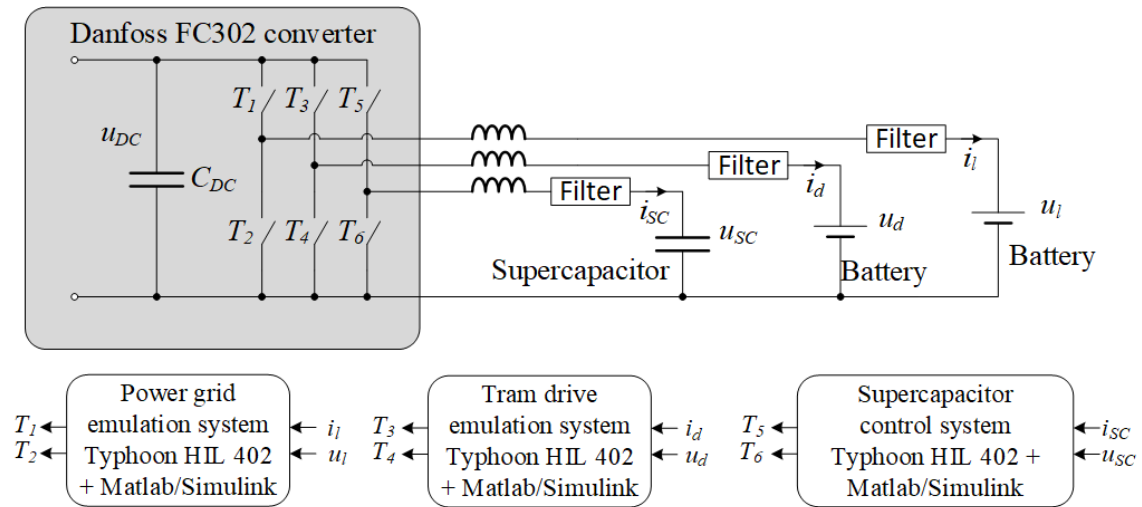


Figure 14. Structure of the HIL laboratory setup.

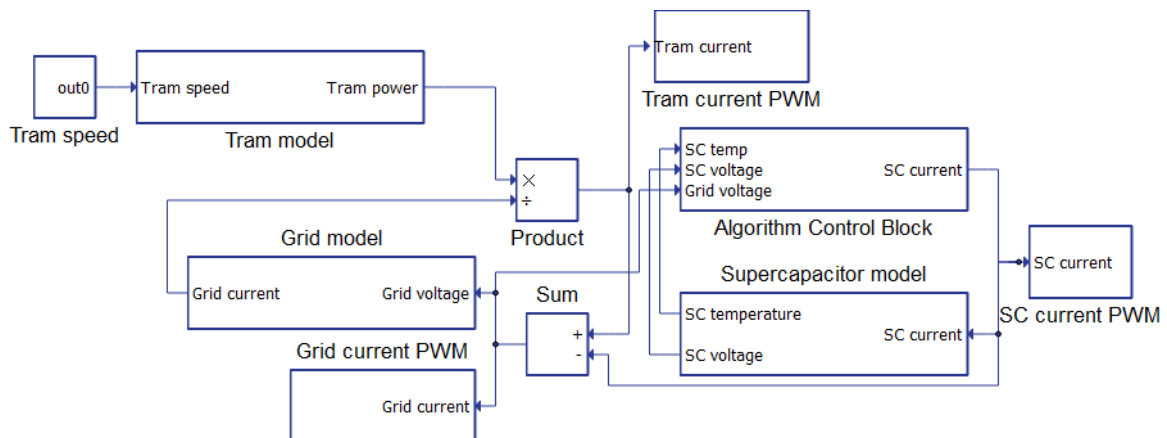


Figure 15. Simulation model within the Typhoon HIL programming environment.

For the experiment, a scaling of the values of the voltage, current, and power of the real system is conducted in order to not exceed the recommended maximum values for the LiFePO₄ batteries, Maxwell supercapacitor, and the Danfoss FC 302 converter. Since the maximum continuous charging current of the batteries is 4 A, the maximum current value flowing through each converter phase was scaled down from 1000 A to 4 A. The supercapacitors and batteries used in the experiment are oversized, meaning that the voltage waveforms have a very slow dynamic compared to their real counterpart, consequently disabling the ability for voltage control. This is why this HIL experiment is only conducted on the basis of the calculated currents and voltages of the SC; the tram and the power grid currents are set as reference values within the model in order for the control algorithm’s calculations along with the coefficient of the algorithm. The lack of emulated voltage control does not impact the validity of the results since the measurements of electric currents are used as inputs to the model within the HIL simulation environment, thus calculating the power grid and tram voltages necessary for the functioning of the control algorithm.

C_{1-HIL} , q_{2-HIL}^0 , and K_{T-HIL} have the same values as their offline MATLAB simulation counterpart. The actual setup is shown in Figure 16 and Table 4 contains the HIL simulation parameters.



Figure 16. HIL simulation emulation setup: 1—autotransformer; 2—Danfoss FC302 converter; 3—Typhoon HIL 402; 4, 5—LiFePO₄ batteries; 6—Maxwell BMOD0083 P048 B01 supercapacitor; 7—Fluke multimeter.

Table 4. HIL simulation parameters.

Parameter	Value	Parameter	Value
C_{SC-HIL}	83 F	R_{th-HIL}	0.04 °C/W
$C_{Bat-HIL}$	12 Ah	C_{th-HIL}	7700 J/°C
U_{SC-HIL}	48 V	$T_{amb-HIL}$	25 °C
$U_{Bat-HIL}$	36 V	$u_{SC0-HIL}$	33 V
R_{l-HIL}	0.0387 Ω	C_{1-HIL}	12,960
L_{l-HIL}	0.0023 H	q_{2-HIL}^0	20
$R_{esr-HIL}$	0.018 Ω	K_{T-HIL}	13,058
f_{SW}	10 kHz		

5.2. HIL Simulation Experiment Results

The experiment was carried out on the basis of the speed profile described in Section 4.1. Real-time measurements of the currents in the SC and in the tram were carried out on the laboratory model and the denormalized results were compared with the offline simulation results from Section 4.1 (Figures 17 and 18).

These experimental results demonstrate the feasibility of the energy storage system for regenerative braking of a rail vehicle using the SC ESS with the proposed energy flow control algorithm. The results obtained from the HIL experiment show the validity of using the presented algorithm in an SC ESS. This creates the basis for a prototype with real electric power values to be used in a rail vehicle and eventually put into production.

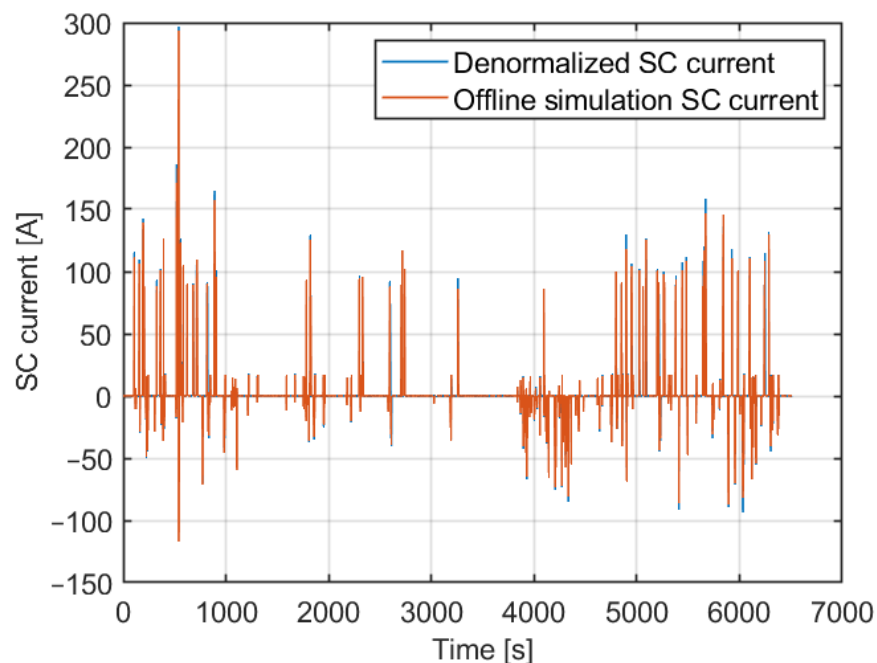


Figure 17. Denormalized SC current obtained from HIL experiment compared to SC current obtained from offline simulation.

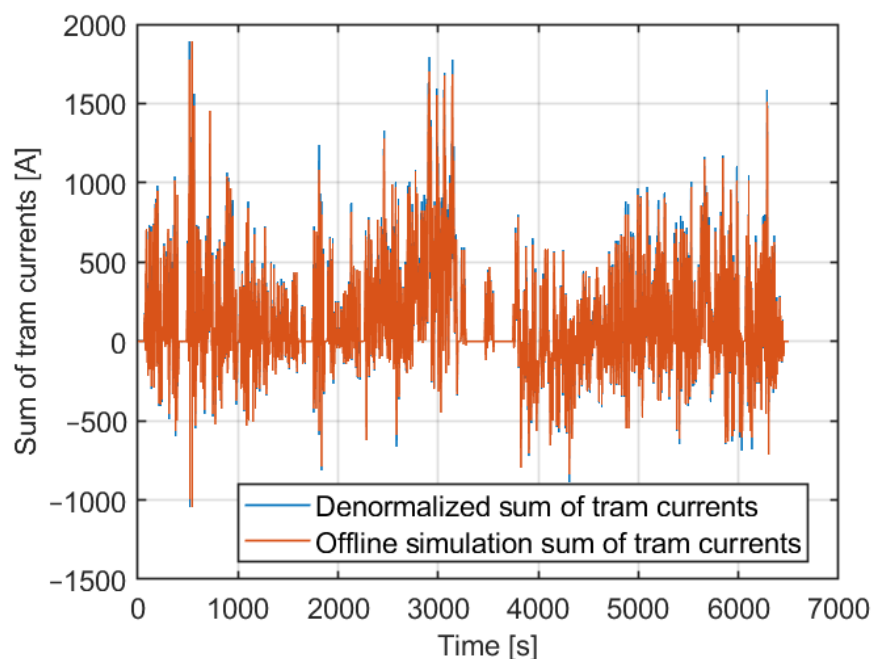


Figure 18. Denormalized sum of tram currents obtained from HIL experiment compared to sum of tram currents obtained from offline simulation.

6. Conclusions

This paper presents a regenerative braking energy flow control algorithm designed for power grid voltage stabilization in tram vehicles with a mobile supercapacitor ESS. This concept of power grid voltage stabilization takes place at times when other vehicles in the vicinity have a negative influence on the power grid voltage value, the acceleration of the considered tram is zero, and the SC is able to exchange energy with the power grid. The SC receives energy from the grid when other vehicles in the vicinity increase the voltage of the power grid by braking and releases energy to the grid when other vehicles reduce

the voltage of the power grid by accelerating, thereby stabilizing the power grid voltage fluctuations caused by other vehicles. The developed algorithm calculates the optimal waveform of the SC current based on Pontryagin's minimum principle, minimizing the difference between the instantaneous value and the ideal voltage value of the power grid, but also minimizing the final temperature of the SC to maximize the lifetime of the SC. The algorithm was tested with an offline simulation experiment in the MATLAB/Simulink programming environment and then experimentally validated with an HIL simulation experiment on the Typhoon HIL402 device using an emulation laboratory setup. It is shown that the proposed algorithm within the tram regenerative braking system successfully reduces the influence of other vehicles on the power grid voltage; it shows a reduction of up to 25% in the amount of the criterion function during a trip and a reduction of up to 17.6% in the voltage deviation of the power grid by using one SC ESS on one vehicle. It was also shown that $8.14 \cdot 10^3$ J of energy can be saved during a journey on the line under consideration. The amount of energy saved depends on the choice of the coefficient K_T , which can be used to emphasize the influence of the algorithm on the total energy saved or on the final temperature, which has a direct impact on the lifetime of the SC. The SC temperature changes during the algorithm's operation are minimal, indicating that the algorithm is suited to be used in conjunction with algorithms that operate only during acceleration and braking. The simulation results obtained form the basis for continuing the research, i.e., future work involves testing the effectiveness of the proposed algorithm under real conditions on a tram.

Author Contributions: I.Ž.: conceptualization, methodology, software, validation, investigation, data curation, writing—original draft preparation, visualization; V.Š.: conceptualization, validation, resources, writing—review and editing, supervision; Ž.B.: conceptualization, methodology, validation, resources, writing—review and editing, supervision; B.N.: validation, software, writing—review and editing, supervision. All authors have read and agreed to the published version of the manuscript.

Funding: This research received no external funding.

Data Availability Statement: The datasets presented in this article are not readily available because they are based on measurements used obtained by a private company. Requests to access the datasets should be directed to authors who can then discuss with the appropriate parties to allow data sharing.

Acknowledgments: The authors would like to express their gratitude to Typhoon HIL Inc. for graciously lending the Typhoon HIL402 real-time hardware-in-the-loop system and the appropriate software, as well as for their technical support during the algorithm validation phase of the paper.

Conflicts of Interest: The authors declare no conflicts of interest.

Nomenclature

The used nomenclature is listed by order of appearance, as follows:

ESS	Energy storage system	$J(\cdot)$	Criterion function
SC	Supercapacitor	K_T	Temperature criterion scaling coefficient
HIL	Hardware in the loop	H	Hamiltonian
$v(t) \equiv v$	Tram speed	$(\cdot)^o$	Optimal value
$p(t) \equiv p$	Tram power	$\lambda(t) \equiv \lambda$	Lagrange multiplier
$u_l(t) \equiv u_l$	Grid voltage	q^o	Normal cone vector
$i_d(t) \equiv i_d$	Tram current	C_1	Differential equation coefficient
$u_{SC}(t) \equiv u_{SC}$	SC voltage	$i_{SC}^o(t) \equiv i_{SC}^o$	Optimal SC current
$T_{SC}(t) \equiv T_{SC}$	SC temperature	K_{SC}	SC current scaling coefficient
$I_{SC_{ref}}(t) \equiv I_{SC_{ref}}$	SC reference current	C_{SC-HIL}	HIL simulation SC capacitance
$i_l(t) \equiv i_l$	Grid current	$C_{Bat-HIL}$	HIL simulation battery capacity

$F_v(t) \equiv F_v$	Total traction force	U_{SC-HIL}	HIL simulation SC nominal voltage
m	Tram mass	$U_{Bat-HIL}$	HIL simulation battery nominal voltage
$a(t) \equiv a$	Tram acceleration	R_{l-HIL}	HIL simulation grid resistance
g	Gravitational constant	L_{l-HIL}	HIL simulation grid inductance
$\alpha(t) \equiv \alpha$	Track inclination	$R_{esr-HIL}$	HIL simulation SC equivalent series resistance
A, B, C	Davis formula coefficient	f_{SW}	HIL simulation switching frequency
U_G	DC voltage source value	R_{th-HIL}	HIL simulation SC thermal resistance
R_l	Grid resistance	C_{th-HIL}	HIL simulation SC thermal capacitance
L_l	Grid inductance	$T_{amb-HIL}$	HIL simulation ambient temperature
C_{SC}	SC capacitance	$u_{SC0-HIL}$	HIL simulation SC operating voltage
R_{esr}	SC equivalent series resistance		
C_{th}	SC thermal capacitance		
R_{th}	SC thermal resistance		
T_{amb}	Ambient temperature		
$P_{loss}(t) \equiv P_{loss}$	SC heat loss		

References

- Commission Regulation (EU) 2019/1781, Official Journal of the European Union, L 272, 25 October 2019. Available online: <https://eur-lex.europa.eu/eli/reg/2019/1781/oj/eng> (accessed on 27 November 2024).
- Popescu, M.; Bitoleanu, A. A Review of the Energy Efficiency Improvement in DC Railway Systems. *Energies* **2019**, *12*, 1092. [CrossRef]
- González-Gil, A.; Palacin, R.; Batty, P. Sustainable urban rail systems: Strategies and technologies for optimal management of regenerative braking energy. *Energy Convers. Manag.* **2013**, *75*, 374–388. [CrossRef]
- Khodaparastan, M.; Mohamed, A.A.; Brandauer, W. Recuperation of Regenerative Braking Energy in Electric Rail Transit Systems. *IEEE Trans. Intell. Transp. Syst.* **2019**, *20*, 2831–2847. [CrossRef]
- Krishan, O.; Suhag, S. An updated review of energy storage systems: Classification and applications in distributed generation power systems incorporating renewable energy resources. *Int. J. Energy Res.* **2019**, *43*, 6171–6210. [CrossRef]
- Li, J.; Xin, D.; Wang, H.; Liu, C. Application of Energy Storage System in Rail Transit: A Review. In Proceedings of the 2022 International Conference on Power Energy Systems and Applications (ICoPESA), Singapore, 25–27 February 2022; pp. 539–552. [CrossRef]
- Liu, X.; Li, K. Energy storage devices in electrified railway systems: A review. *Transp. Saf. Environ.* **2020**, *2*, 183–201. [CrossRef]
- Zhao, J.; Burke, A.F. Review on supercapacitors: Technologies and performance evaluation. *J. Energy Chem.* **2021**, *59*, 276–291. [CrossRef]
- Yadlapalli, R.T.; Alla, R.R.; Kandipati, R.; Kotapati, A. Super capacitors for energy storage: Progress, applications and challenges. *J. Energy Storage* **2022**, *49*, 104194. [CrossRef]
- Liu, S.; Wei, L.; Wang, H. Review on reliability of supercapacitors in energy storage applications. *Appl. Energy* **2020**, *278*, 115436. [CrossRef]
- Wu, C.; Lu, S.; Tian, Z.; Xue, F.; Jiang, L. Energy-Efficient Train Control with Onboard Energy Storage Systems considering Stochastic Regenerative Braking Energy. *IEEE Trans. Transp. Electrif.* **2024**, *10*, 8275–8286. [CrossRef]
- Sumpavakup, C.; Ratniyomchai, T.; Kulworawanichpong, T. Optimal energy saving in DC railway system with on-board energy storage system by using peak demand cutting strategy. *J. Mod. Transp.* **2017**, *25*, 223–235. [CrossRef]
- Liu, W.; Xu, J.; Tang, J. Study on control strategy of urban rail train with on-board regenerative braking energy storage system. In Proceedings of the 43rd Annual Conference of the IEEE Industrial Electronics Society, Beijing, China, 29 October–1 November 2017; pp. 3924–3929. [CrossRef]
- Pavlović, T.; Župan, I.; Šunde, V.; Ban, Ž. HIL Simulation of a Tram Regenerative Braking System. *Electronics* **2021**, *10*, 1379. [CrossRef]
- Radu, P.V.; Szelag, A.; Steczek, M. On-Board Energy Storage Devices with Supercapacitors for Metro Trains—Case Study Analysis of Application Effectiveness. *Energies* **2019**, *12*, 1291. [CrossRef]
- Zhang, B.; Lu, S.; Peng, Y.; Wu, C.; Meng, G.; Feng, M.; Liu, B. Impact of On-Board Hybrid Energy Storage Devices on Energy-Saving Operation for Electric Trains in DC Railway Systems. *Batteries* **2022**, *8*, 167. [CrossRef]
- Zhang, B.; Wu, C.; Meng, G.; Xue, F.; Lu, S. Optimal Sizing of Onboard Hybrid Energy Storage Devices Considering the Long-Term Train Operation. *IEEE Access* **2022**, *10*, 58360–58374. [CrossRef]

18. Zhong, Z.; Yang, Z.; Fang, X.; Lin, F.; Tian, Z. Hierarchical Optimization of an On-Board Supercapacitor Energy Storage System Considering Train Electric Braking Characteristics and System Loss. *IEEE Trans. Veh. Technol.* **2020**, *69*, 2576–2587. [[CrossRef](#)]
19. Lamedica, R.; Ruvio, A.; Palagi, L.; Mortelliti, N. Optimal Siting and Sizing of Wayside Energy Storage Systems in a D.C. Railway Line. *Energies* **2020**, *13*, 6271. [[CrossRef](#)]
20. Kampeerawat, W.; Koseki, T. A strategy for utilization of regenerative energy in urban railway system by application of smart train scheduling and wayside energy storage system. *Energy Procedia* **2017**, *138*, 795–800. [[CrossRef](#)]
21. Allen, L.; Chien, S. Application of Regenerative Braking with Optimized Speed Profiles for Sustainable Train Operation. *J. Adv. Transp.* **2021**, *2021*, 8555372. [[CrossRef](#)]
22. Tostado-Véliz, M.; Arévalo, P.; Jurado, F. An optimization framework for planning wayside and on-board hybrid storage systems for tramway applications. *J. Energy Storage* **2021**, *43*, 103207. [[CrossRef](#)]
23. Zhao, S.; Feng, Q.; Yang, H.; Zhang, Y. Control strategy of hybrid energy storage in regenerative braking energy of high-speed railway. *Energy Rep.* **2022**, *8*, 1330–1338. [[CrossRef](#)]
24. Che, C.; Wang, Y.; Lu, Q.; Peng, J.; Liu, X.; Chen, Y.; He, B. An effective utilization scheme for regenerative braking energy based on power regulation with a genetic algorithm. *IET Power Electron.* **2022**, *15*, 1392–1408. [[CrossRef](#)]
25. Sengor, I.; Kilickiran, H.C.; Akdemir, H.; Kekezoglu, B.; Erdinc, O.; Catalao, J.P.S. Energy Management of a Smart Railway Station Considering Regenerative Braking and Stochastic Behaviour of ESS and PV Generation. *IEEE Trans. Sustain. Energy* **2018**, *9*, 1041–1050. [[CrossRef](#)]
26. Qin, Q.; Guo, T.; Lin, F.; Yang, Z. Energy Transfer Strategy for Urban Rail Transit Battery Energy Storage System to Reduce Peak Power of Traction Substation. *IEEE Trans. Veh. Technol.* **2019**, *68*, 11714–11724. [[CrossRef](#)]
27. Kleftakis, V.A.; Hatziargyriou, N.D. Optimal Control of Reversible Substations and Wayside Storage Devices for Voltage Stabilization and Energy Savings in Metro Railway Networks. *IEEE Trans. Transp. Electrification* **2019**, *5*, 515–523. [[CrossRef](#)]
28. Roch-Dupré, D.; Gonsalves, T.; Cucala, A.P.; Pecharromán, R.R.; López-López, Á.J.; Fernández-Cardador, A. Determining the optimum installation of energy storage systems in railway electrical infrastructures by means of swarm and evolutionary optimization algorithms. *Int. J. Electr. Power Energy Syst.* **2021**, *124*, 106295. [[CrossRef](#)]
29. Župan, I.; Šunde, V.; Ban, Ž.; Novoselnik, B. An Energy Flow Control Algorithm of Regenerative Braking for Trams Based on Pontryagin’s Minimum Principle. *Energies* **2023**, *16*, 7346. [[CrossRef](#)]
30. Negroiu, R.; Ionescu, C.; Svasta, P.; Vasile, A. Influence of temperature on supercapacitors behavior in series/parallel connections. In Proceedings of the 2017 IEEE 23rd International Symposium for Design and Technology in Electronic Packaging (SIITME), Constanta, Romania, 26–29 October 2017; pp. 367–370. [[CrossRef](#)]
31. Reichbach, N.; Mellincovsky, M.; Peretz, M.M.; Kuperman, A. Long-Term Wide-Temperature Supercapacitor Ragone Plot Based on Manufacturer Datasheet. *IEEE Trans. Energy Convers.* **2016**, *31*, 404–406. [[CrossRef](#)]
32. Sengor, I.; Kilickiran, H.C.; Akdemir, H.; Kilic, B. Determination of Potential Regenerative Braking Energy in Railway Systems: A Case Study for Istanbul M1A Light Metro Line. *J. Autom. Control Eng.* **2017**, *5*, 21–25. [[CrossRef](#)]
33. Župan, I.; Šunde, V.; Ban, Ž.; Krušelj, D. Algorithm with temperature-dependent maximum charging current of a supercapacitor module in a tram regenerative braking system. *J. Energy Storage* **2021**, *36*, 102378. [[CrossRef](#)]

Disclaimer/Publisher’s Note: The statements, opinions and data contained in all publications are solely those of the individual author(s) and contributor(s) and not of MDPI and/or the editor(s). MDPI and/or the editor(s) disclaim responsibility for any injury to people or property resulting from any ideas, methods, instructions or products referred to in the content.